Published in final edited form as:
J Pharm Sci. 2009 September ; 98(9): 3218–3238. doi:10.1002/jps.21768.

Monoclonal Antibody Interactions with Micro- and Nanoparticles: Adsorption, Aggregation and Accelerated Stress Studies

Jared S. Bee[1], **David Chiu**[1], **Suzanne Sawicki**[1], **Jennifer L. Stevenson**[2], **Koustuv Chatterjee**[2], **Erwin Freund**[2], **John F. Carpenter**[3], and **Theodore W. Randolph**[1]

[1] Department of Chemical and Biological Engineering, University of Colorado, Boulder, Colorado 80309

[2] Drug Product & Device Development, Amgen Inc., Thousand Oaks, CA 91320

[3] Department of Pharmaceutical Sciences, University of Colorado Health Sciences Center, Denver, Colorado 80262

Abstract

Therapeutic proteins are exposed to various wetted surfaces that could shed sub-visible particles. In this work we measured the adsorption of a monoclonal antibody (mAb) to various microparticles, characterized the adsorbed mAb secondary structure, and determined the reversibility of adsorption. We also developed and used a front-face fluorescence quenching method to determine that the mAb tertiary structure was near-native when adsorbed to glass, cellulose and silica. Initial adsorption to each of the materials tested was rapid. During incubation studies, exposure to the air-water interface was a significant cause of aggregation but acted independently of the effects of microparticles. Incubations with glass, cellulose, stainless steel or Fe_2O_3 microparticles gave very different results. Cellulose preferentially adsorbed aggregates from solution. Glass and Fe_2O_3 adsorbed the mAb but did not cause aggregation. Adsorption to stainless steel microparticles was irreversible, and caused appearance of soluble aggregates upon incubation. The secondary structure of mAb adsorbed to glass and cellulose was near-native. We suggest that the protocol described in this work could be a useful preformulation stress screening tool to determine the sensitivity of a therapeutic protein to exposure to common surfaces encountered during processing and storage.

Keywords

protein aggregation; adsorption; microparticles; surface chemistry; stability; processing; biotechnology; fluorescence spectroscopy; monolayer; monoclonal antibody

INTRODUCTION

Protein aggregates have caused immune responses in patients treated with several different therapeutic protein products.1 Consequences of these immune responses can include loss of product efficacy, anaphylactic shock or generation of cross-reactive antibodies that can neutralize both the therapeutic and the endogenous protein.2⁻4 The size of protein aggregates and the conformation of the proteins comprising aggregates are thought to be critical to their immunogenicity.3 Currently, it is proposed that large aggregates composed

Correspondence to: Theodore W. Randolph (Telephone: 303-492-4776); Theodore.Randolph@colorado.edu; Fax: 303-492-4341).

of highly ordered arrays of near-native proteins are potentially the most immunogenic.[2–4] Proteins can aggregate during processing, shipping, storage and delivery to the patient. Formulation conditions are chosen to maximize protein stability over its shelf-life. However, even thermodynamically and colloidally stable proteins may aggregate after interaction with the container-closure system, container leachates, or particulate contaminants because the stability with respect to surfaces may involve different physical processes than those that determine stability in bulk solution.[5,6]

There are many documented cases in which the interaction of a therapeutic protein with container-closure materials, delivery devices or process-related contaminants caused aggregation or loss of activity. For example: recombinant human platelet-activating factor acetylhydrolase aggregation was nucleated by silica nanoparticles;[5] Teflon® caused aggregation of insulin;[7] silicone rubber delivery tubing decreased interleukin-2 activity by 97%;[8] adsorption of Factor VIII onto PVC infusion bags reduced its activity by 42%;[9] silicone oil syringe lubricant induced aggregation of several model proteins;[10] leachates from tungsten caused protein precipitation;[11,12] stainless steel particles shed from a filler pump in the laboratory environment caused aggregation of a mAb;[13] and Teflon® containers fostered aggregation of an IgG_2, during freeze-thawing.[14]

The container-closure is not the only material to contact the protein after the final sterile filtration operation. After filtration, the protein solution contacts the wetted surfaces of pump and tubing materials during the filling of the container-closure system. After contact with the surfaces of the container-closure during storage and shipping, it is finally exposed to product contact surfaces in the delivery systems, e.g. IV bags and lines, and needles. All product contact surfaces are potential sources of leachable or particulate foreign materials. For example, Ennis *et al.* demonstrated that the sterilization of glass vials can result in delamination of glass microparticles from the inner surface of vials into the bulk of parenteral pharmaceuticals.[15] Akers and Nail concluded that particulate contamination of parenterals from glass vials is unavoidable regardless of the quality of glass.[16] Because sub-visible heterogeneous particles may be present in the final product they could nucleate aggregation and the appearance visible particulates upon storage. Stainless steel, glass and cellulose are examples of some of the many materials to which biopharmaceuticals are exposed. Surface- or particle-induced aggregation of proteins could be modulated by changes in process (such as filtering), changes in product contact surfaces (containers, process equipment), or changes in formulation (types and levels of excipients).[17] Although accelerated degradation studies with respect to temperature and agitation are routinely performed in formulation development, and tests are performed in the final container-closure and delivery materials, accelerated formulation stability testing or stress testing that specifically focuses on particle contamination is not currently commonplace.

In this work we investigated the effects of exposure of a monoclonal antibody (mAb) to glass, cellulose or stainless steel microparticles, and characterized the resulting protein aggregation. These materials were chosen because of their widespread use in biopharmaceutical production. We also studied the mAb interaction with iron(III) oxide (Fe_2O_3), titania (TiO_2), alumina (Al_2O_3) and silica (SiO_2). Fe_2O_3 was studied because it is a major component in rust that allows a comparison with results using passivated stainless steel which displays a chromium oxide surface. The titania, alumina and silica particles were chosen to obtain data covering a wider range of surface charge (inferred from the ζ-potential) and because of the potential applications of our methods for studying systems germane to medical implants (titania), vaccine-adjuvants (alumina), and immobilized enzymes (silica). Nanoparticles of silica and alumina were studied to investigate the effect of primary particle size. Our methods and results are applicable to other systems that are outside of the scope of this work: we note that artificial implants have the potential for

shedding particles (up to 10^{12} nanoparticles/year) into the body[18,19] and particulates that enter the body through other means both could bind and interact in unexpected ways with proteins in the patient (for a review see[20]).

Microparticle surfaces could exert multiple effects on proteins. Protein molecules may adsorb to microparticles, which in turn may stimulate aggregation in the bulk solution or allow for formation of larger particles resulting from multilayer protein adsorption, or agglomeration of colloidally-destabilized protein-coated-particles. If a surface does cause aggregation, by analogy with Lumry-Eyring models for aggregation in bulk solution,[5,21] we hypothesize that a necessary first step for aggregation may be partial unfolding of the protein on the surface. Aggregation could then be propagated by partially folded protein molecules on the surface or by those protein molecules that desorb back into the bulk solution. It is not currently known if surface exposure is a major causative factor in the aggregation of formulated therapeutic monoclonal antibodies. The overall aims of this research were to gain fundamental insights into the adsorption of a mAb to microparticles and the effects of this interaction on protein structure and aggregation, and to develop an accelerated stability protocol that could have practical uses to isolate, identify and replicate microparticle- and surface-induced particle formation or aggregation.

MATERIALS AND METHODS

Materials

The model monoclonal antibody (mAb) used in these studies was a humanized immunoglobulin-G_1 (IgG_1) antistreptavidin donated by Amgen Inc. (Thousand Oaks, CA). This mAb is not a commercial or development product. This mAb formulated in 10 mM sodium acetate, pH 5.0 (“buffer”) was used in experiments except where otherwise noted. The properties of the IgG mAb are as follows: molecular weight, M = 145 kDa (including 3 kDa glycosylation); UV extinction coefficient, $\varepsilon = 1.586$ mL/mg·cm; isoelectric point, pI = 8.7; and hydrodynamic diameter, $D_h = 10.5 \pm 0.5$ nm. This mAb solution contained ~ 2% dimer as received. The ζ-potential of the mAb in 10 mM sodium acetate buffer (pH 5.0) was measured as $+12.1 \pm 0.4$ mV.

The following materials were obtained from Sigma-Aldrich (St. Louis, MO) and were heated in air at 425°C for 4 hours to remove any potential volatile surface contaminatants and then stored in a dessicator: iron(III) oxide, powder, <5 micron, 99+%; silicon dioxide, 0.5–10 μm, approx. 99%,; silica, nanopowder, particle size 15 nm, 99.5%; aluminum oxide powder, <10 μm, 99.7% (alumina); aluminum oxide nanopowder, particle size 47 nm; titanium(IV) oxide powder, < 5 μm, 99.9+%, rutile (titania). Sigmacell® Cellulose, Type 20 (20 μm) was obtained from Sigma-Aldrich (St. Louis, MO) and used without further processing. All other chemicals not specifically mentioned were of reagent grade or higher quality.

Stainless Steel Microparticles

Stainless steel microparticles (P316L grade) were donated by Ametek, Inc. (Eighty Four, PA). According to the manufacturer, the stainless steel microparticles were produced by exposure of molten steel to water. The material contained 80% smaller than a 400-mesh microparticles and the process of “water atomization” produces a relatively thick oxide coating (Ametek product information).

Stainless Steel Microparticles Passivation and Passivation Testing

Stainless steel surfaces of equipment used in the biotechnology industry are frequently passivated to reduce levels of ‘free iron’ that may lead to rusting of the surface; passivation

produces a corrosion-resistant chromium oxide-rich surface.22,23 To test the effects of passivation treatment on interactions of the protein with stainless steel surfaces, we followed a passivation treatment that corresponds to ASTM A-967-05 Part 7 and ASTM A-380-06.22,23 Passivated stainless steel microparticles were prepared by incubating the stainless steel microparticles in a 1% v/v Tergitol NP-9® for 30 minutes at approximately 50°C. The steel was then washed in a 3% w/v citric acid solution for 2 hours at 50°C, followed by adjustment of the pH to 8.0 by addition of triethanolamine. Finally, the steel was incubated in a 25% w/v sodium nitrate solution for 30 minutes at room temperature, then thoroughly rinsed with purified water and dried over acetone. The stainless steel microparticles passed the ASTM A-967-05 Practice D - Copper Sulfate Test for passivation both before and after the passivation treatment was performed. The stainless steel microparticle properties (BET surface area, particle size distribution and ζ-potential) were re-measured after the passivation treatment was performed.

Ground Glass Microparticles

Glass microparticles were prepared from vials (Vial, 5 cc, Blowback, Type 1 Glass, USP/PhEur, Non-treated; P/N 2705B80B, Alcan Packaging, Syracuse, NE) and syringe barrels (formed borosilicate glass blanks, Becton Dickinson, Franklin Lakes, NJ) by ball-milling broken glass shards with zirconia (ZrO_2) ball-grinding media and sieving with a 63 μm screen. Elemental analysis after grinding showed that the ground glass vials and ground glass syringes were surface-contaminated with Zr from the grinding media at 375 ppm and 13 ppm respectively.

ISO 4802-2 defines borosilicate glass as containing between 5 and 13 % boric oxide (B_2O_3) and neutral glass as also containing 5 and 13 % boric oxide (B_2O_3) but with additional aluminum and/or alkaline earth oxides content (Al_2O_3, CaO, Na_2O, K_2O).24 Glass may also contain other trace impurities. The freshly exposed glass surface after grinding may have different surface levels of Na_2O, K_2O, and CaO compared to unground glass. These oxides can potentially leach alkalinity, causing pH shifts in stored protein formulations. To reduce this effect, ground glass vials were washed with 1 M ammonium sulfate and thoroughly rinsed with purified water to dissolve and wash away the exposed oxides. Finally, they were dried under vacuum at 105 °C, and the dried cake gently broken with a mortar and pestle. After processing, the microparticle properties (surface area, particle size distribution and ζ-potential) were re-measured.

Relative Hydrolytic Stability Testing of Ground Glass Microparticles

Hydrolytic stability of microparticles from vials, syringes and sulfate-washed microparticles was compared using an adaptation of ISO 4802-2 test for glass hydrolytic stability. Hydrolytic stability refers to the release of Na, K, and Ca ions from their oxides present on the glass surface after autoclaving at 121°.24 We adapted the standard protocol (designed for whole containers) for the glass microparticles we used in our work. A sample of about 200 mg of each ground glass type was dispersed into 10.00 mL of water and the sample was autoclaved for 30 min at 121 °C. After autoclaving, the samples were centrifuged. The supernatant was analyzed three times for Na, Ca, and K using ICP-OES and results were compared with water blanks prepared without addition of microparticles.

The results of this analysis showed that for all samples K and Ca were below the instrument detection limit. Ground glass microparticles from vials, syringes, and sulfate-washed microparticles released 70 ± 2 ppm, 60 ± 1 ppm, and 30 ± 1 ppm of Na respectively. We can estimate that the surface area-to-volume in a whole pre-filled syringe or vial is ~ 10 cm^2/mL or less. In our procedure we tested ground glass at ~ 1000 cm^2/mL, so division of our results by ~ 100 should reasonably correlate to whole-vial test results. Our results are consistent

with the ground glass having extremely high hydrolytic stability (HC1/HC2 classification < 5 ppm).24 The sulfate-washing procedure did further increase the hydrolytic stability, but this procedure is probably not necessary for accelerated stability testing of mAb with ground glass (although we still tested it in this work).

Particles and mAbζ-Potentials

The ζ-potential of particles and mAb in 10 mM sodium acetate buffer (pH 5.0) was measured with a Zetasizer® Nano-ZS (Malvern Instruments Ltd, UK). In samples containing a significant fraction of microparticles with a size above 10 μm, the particles were allowed to settle before measurement so as not to exceed the instrument measurement range. The mAb concentration was about 2 mg/mL, and the mAb result is reported in the materials section description of the mAb properties.

Particle Surface Area and Size Distribution

Particle specific surface area was determined using nitrogen adsorption and Brunauer-Emmett-Teller (BET) isotherm analysis using an Autosorb 1C (Quantachrome Instruments, Boynton Beach, FL). The results for stainless steel microparticles, which exhibited specific surface areas at the low end of the instrument range for nitrogen BET analysis were verified with a krypton gas measurement.

The size distribution of a microparticle suspension in buffer (and diluted in pure water during the measurement) was measured three times using a Coulter LS230 light scattering instrument (Beckman Coulter Inc., Miami, FL) and reported as the mean surface area-weighted size.

The size distribution of nanoparticles was measured using the dynamic light scattering function of the Zetasizer® Nano-ZS.

Scanning Electron Microscopic Analysis

Scanning electron microscopy (SEM) was used to obtain images of particles for qualitative evaluation of their morphologies. Samples were mounted on carbon tape and sputter-coated with gold (~ 3 nm coating). Images were collected with a JSM-6480LV (JEOL Ltd., Tokyo, Japan) SEM instrument.

Elemental Analysis

Inductively coupled plasma optical emission spectrometry (ICP-OES) using an ARL 3410+ (Thermo Fisher Scientific, Inc., Waltham, MA) was used for elemental analysis. Contamination from the zirconia grinding media was measured by performing a sulfuric acid surface wash of the ground glass. Metal ion extractables from glass were measured in the supernatant generated in performing the hydrolytic stability extraction process. Results of hydrolytic stability are reported in description of the glass materials.

Protein and Soluble Aggregate Assays

Size exclusion chromatography (SEC) was used to quantify mAb monomer and soluble aggregate levels. SEC was performed with a TSK-GEL G3000SW_{XL} column and SW guard column (Tosoh Bioscience LLC, Montgomeryville, PA). A 126 pump (Beckman Coulter Inc., Fullerton, CA) and a Waters 717 Plus autosampler (Waters Corp., Milford, MA) were used. The mobile phase consisted of 100 mM sodium phosphate, 300 mM sodium chloride, and 0.01% w/v sodium azide (pH 7.0), and the flow rate was 0.6 mL/min. Protein was detected using a Beckman Gold 166 UV detector at 280 nm.

Adsorption of mAb to Microparticles

The amount of mAb adsorbed to microparticles was determined by depletion of protein from solution after mixing with particles and performing a mass balance. A stock suspension of microparticles in buffer was prepared (for stainless steel the particles were directly weighed into 1.7 ml polypropylene microcentrifuge tubes). Samples were prepared by mixing buffer, the microparticle suspension, and a stock mAb solution to yield samples with a constant final protein concentration of between 0.1 and 0.2 mg/mL in a total volume of 0.5 mL, and a range of microparticle concentrations. The solutions were incubated at 4–8°C for 30 min with mixing by end-over-end rotation in 1.7 mL polypropylene microcentrifuge tubes at 8 rotations per minute. Samples were then centrifuged to clarity for 5–30 min at 12,000 ×g, and the supernatant was assayed for protein content by SEC. Triplicate tubes were prepared and analyzed for each sample conditions. The fraction of mAb monomer remaining in solution was plotted versus the microparticle surface area added per milligram of protein and extrapolated to the x-axis intercept to find the apparent surface area occupied per mg mAb ("mAb footprint") on each microparticle type. Adsorption experiments with silica showed that between 5 min and 1 hour of mixing gave essentially the same results, suggesting that adsorption was essentially complete within 5 minutes.

In experiments with stainless steel microparticles we observed formation of soluble mAb aggregates. To determine if leachates from the stainless steel microparticles were responsible for the observed protein aggregation we dispersed in buffer a mass of steel microparticles equivalent to the highest levels used in adsorption experiments (556 mg/mL of steel). The dispersion was incubated for 30 min at 4–8 C and then centrifuged 12,000 ×g for 5 min. The supernatant was collected and recentrifuged at 12,000 ×g for 30 min. An aliquot (450 μL) of the final supernatant was mixed with 50 μL of mAb at 1 mg/mL, incubated for 30 min, and finally analyzed by SEC.

Reversibility of mAb Adsorption

Reversibility of adsorption was assessed by dilution of samples of microparticles in buffer. Microparticles with adsorbed mAb were centrifuged and then resuspended in 3× the original sample volume of sodium acetate buffer (pH 5.0), incubated for an additional 30 min and then re-centrifuged. The final sample supernatant was analyzed for desorbed protein using SEC. Mass balances were used to evaluate reversibility of mAb adsorption to glass (vials), cellulose and stainless steel microparticles.

To determine whether adsorbed mAb might be released from microparticles *in vivo*, we examined desorption following resuspension of centrifuged particles containing adsorbed protein in phosphate buffered saline (137 mM NaCl, 10 mM phosphate and 2.7 mM KCl at pH 7.4, PBS), a solution representative of extracellular fluid pH and salt content but without proteins. Reversibility of adsorption was tested by collecting the initial pellet as above and resuspending it in the initial volume (0.5 mL) of PBS, followed by re-incubation and re-centrifugation as described above. Again, mass balances were used to evaluate reversibility of mAb adsorption to glass, cellulose, and stainless steel microparticles.

Incubation Studies

Based on the results from the adsorption experiments, a quantity of microparticles sufficient to adsorb about 15–25% of the initial 0.1 mg/mL of mAb was used in extended incubation studies in 10 mM sodium acetate buffer (pH 5.0). The pH was measured after addition of microparticles, but because addition of microparticles resulted in at most a 0.1 increase in the pH no further pH adjustment was made.

Two methods were used for incubation studies. In the first method (method A) we overfilled vials to remove the headspace and therefore eliminate the air-water interface. The method of overfilling vials to remove headspace was used to incubate mAb with glass, cellulose, stainless steel and Fe_2O_3 microparticles. This is the main method we recommend for performing accelerated stability studies of protein with respect to effects of microparticles alone. In the second method (method B; used for silica, alumina and titania) we investigated the potential for synergistic effects of microparticles and the air-water interface by performing incubations in vials with headspace.

To allow for the initial adsorption of protein to microparticles, using method A (incubation in overfilled vials without headspace), 1 mL samples of mAb-microparticle dispersions were first prepared and incubated for 30–60 min in 1.7 mL polypropylene microcentrifuge tubes with end-over-end rotation at 8 rpm. Then 0.8 mL of each sample were used to overfill separate 0.6 mL polypropylene microcentrifuge tubes in order to minimize the air-water interface. Triplicate 0.6 mL tubes were prepared for each datum point collected. Some of the 0.6 mL vials contained a residual air bubble up to about 4 mm in diameter after filling. After incubation at 4–8 °C with end-over-end rotation (8 rpm) for various times, each sample was centrifuged for 5–30 min at 12,000 ×g, and the supernatant was assayed by SEC. The sample assay results were compared those for control samples prepared and incubated without microparticles.

Studies using method B (incubation in vials with headspace) were performed over five days in 1.7 mL polypropylene vials filled to 0.5 mL with the mAb and microparticles dispersion. This method of incubation was used for silica, alumina and titania microparticles.

mAb Secondary Structure Analysis using Infrared Spectroscopy

The secondary structures of the native and adsorbed protein were analyzed using infrared spectroscopy of the amide I band. Spectra were acquired on a Bomem MB-series spectrometer (PQ, Canada). A BioCell (BioTools Inc., Jupiter, FL) with CaF_2 windows and a 6.5 μm path length was used to collect 128 single-beam transmission scans at 4 cm^{-1} resolution. Protein absorption spectra were calculated by subtraction of appropriate buffer blank spectra from the sample spectra. The previously published procedures for water vapor noise subtraction was applied if necessary.25 The second derivative of each absorption spectrum was calculated with a 7–11 point Savitsky-Golay function depending upon the data quality. The derivative spectra were then baseline corrected, area-normalized, offset corrected and processed with a 2× fast Fourier transform interpolation function. Spectral quality was assessed according to previously published specifications.25,26 Triplicate samples were analyzed.

Because the cell had a path length of 6.5 μm, we were limited to measuring finer particles. Therefore, all infra-red spectra measurements were made on the fine fraction of particles obtained after settling under gravity. We found that the larger size of the steel microparticles were unsuitable for dispersion between the IR cell surfaces. We suspended microparticles in buffer and allowed the larger particles to settle to obtain a dispersion of the smaller fraction of microparticles. Samples for IR analyis were formed by adding aliquots of the fine particle dispersions to mAb at 1 mg/mL. Sufficient particles were added to adsorb all of the protein as verified by UV absorption of the supernatant. The samples were then centrifuged to form a pellet of particles, which was then re-suspended in fresh buffer. The same process was applied to microparticle dispersions without protein to obtain ‘buffer’ spectra for subtraction and data analysis.

mAb Tertiary Structure Analysis using Tryptophan Fluorescence Quenching

Front-face fluorescence and fluorescence quenching methods were used to probe the tertiary structure of mAb adsorbed to microparticles. Tertiary structure of the mAb was assessed by performing acrylamide quenching of tryptophan (Trp) fluorescence. Surface-exposed Trp are collisionally quenched by acrylamide to a greater extent than buried Trp and therefore can be used to infer relative tertiary structure of the protein.27

Front-face fluorescence measurements of opaque mAb-adsorbed-to-microparticles dispersions were obtained using a triangular cuvette that was securely mounted in the optical path of an SLM-Aminco Spectrofluorometer (SLM-Aminco, Urbana, IL) with an angle of incidence of 53° to avoid the scattering and specular reflection signals. The intensity of the fluorescence signal was strongly dependent upon the exact angle of the cuvette, so the overlay of the long wavelength edge of the excitation scattering was used as a quality check that the cuvette angle had not changed during measurements. Quenching of mAb adsorbed to ground glass vials, ground glass syringes, cellulose microparticles, and silica microparticles was performed. A pipette was used to manually mix the glass and silica dispersions before readings. Settling of glass and silica microparticles during the measurement was found to be negligible as determined by a decrease of less than 1 ± 1% in intensity at 328 nm after 30 s. For cellulose, settling was a problem for manual mixing therefore a small motor was used to drive an impeller in the cuvette to give well-mixed dispersion that did not have a decrease in intensity due to settling. The cuvette was temperature-controlled to 25°C. Comparison measurements of clear protein control solutions (without particles) were obtained using a 1 cm square cuvette and a 90° geometry.

Acrylamide was used to quench the intrinsic tryptophan fluorescence of the mAb, both when free in solution, and when fully bound to microparticles. The protein concentration used was 0.1 mg/mL. In the 90° control measurements an inner-filter effect correction was applied to account for the UV absorption of acrylamide at 295 nm.27 Samples of protein fully bound to microparticles were prepared and incubated with end-over-end rotation at 8 rpm at controlled room temperature (ca. 23°C) for 30–60 min and readings taken at 25°C. Excess microparticles were added so that the mAb surface coverage was only about a quarter of the total available surface (or half for cellulose if it forms a double layer). Protein adsorbed to silica in 10 mM sodium acetate buffer (pH 5.0) was also measured after longer incubations of 1 and 5 days to determine if there were any slower structural changes occurring in the adsorbed protein. A wavelength of 195 nm with a bandwidth of 4 nm was used to excite the tryptophan fluorescence, which was monitored at 328 nm for native and adsorbed protein, 348 nm for protein unfolded in 9 M urea, and 350 nm for NATA. The emission was scanned at 0.95 nm/s from 300–380 nm. Acrylamide was freshly prepared as a 7.88 M stock each day. The measured fluorescence intensities were corrected for dilution from addition of stock acrylamide aliquots before further analysis.

The quenching data for three separate replicate experiments were analyzed using the Stern-Volmer equation:

$$F_0/F=1+K_{sv}[Q] \quad (1)$$

where F_0 and F are the fluorescence intensities in the absence and presence of quencher respectively, [Q] is the quencher concentration (M), K_{SV} is the Stern-Volmer constant (M^{-1}). We compared quenching results for the native mAb in solution, the unfolded mAb in solution, and the mAb adsorbed to the different particles surfaces.

Statistical Tests used in Data Analysis

The statistical T-Test function in Microsoft Excel® was used to evaluate the significance of differences in data sets and reported as a p-value. A p-value of less than 0.05 was interpreted to indicate statistically significant differences in data sets.

RESULTS

Particle Properties

SEM images of dry particles are shown in Figure 1 and the BET specific surface areas for dry particles are given in Table 1. For the particles suspended in aqueous solutions, ζ-potentials and size distributions are given in Table 1. In this work we used these multiple particle characterization techniques because for real-world particles (like ground glass) the size and shapes are far from uniform and the agglomeration state can vary depending upon whether dry or suspended in solution. We also note that the size distribution data from laser diffraction (Coulter LS230 data) was reported in area-weighted statistics (volume and number statistics give different distributions) and the dynamic light scattering data for nanoparticles (zetasizer) was reported in number statistics.

The SEM data show that the morphologies of particles obtained from glass vials, glass vials after the sulfate wash, and glass syringes were similar. The BET data suggest that the sulfate wash increased the specific surface area of the particles obtained from glass vials. Passivation did not appear to change the morphology of the stainless steel particles. The SEM images for Fe_2O_3, titania, alumina nanoparticles and silica nanoparticles show significant agglomeration in the dry form. Comparison of the SEM images and the solution particle size data suggests that the Fe_2O_3, titania, alumina nanoparticles and silica nanoparticles also remained somewhat agglomerated in solution. From these data it is not possible to estimate how strongly agglomerated the primary particles are in solution, but it appears that agglomeration could be a factor in the adsorption results, particularly for alumina nanoparticles, which did not appear to adsorb protein at levels expected based upon added surface area calculated from BET measurements of dry powders.

Adsorption Studies

The adsorption isotherms for the mAb on various particles are shown in Figure 2, panels A–D. The measured footprint determined from the x-axis intercept represents the apparent adsorption footprint of this mAb on each particle type (Table 1). The linearity of the plots (for all but the case of protein adsorbed to cellulose, the data could be fit to straight line linear regressions with a correlation coefficient $r^2 \sim 0.99$) suggests that the adsorption is of relatively high affinity. Slightly more curvature was observed for mAb adsorption to cellulose ($r^2=0.98$), perhaps indicating more reversible adsorption or adsorption of species with multiple affinities. This steady-state experiment did not assess whether there could be any rapid dynamic adsorption or desorption occurring. The apparent footprint for the adsorption of the mAb onto all the microparticles tested in this work fell between 0.3 and 1 m^2/mg (except for alumina nanoparticles, which did not adsorb mAb).

SEC chromatograms showed that mAb dimer levels in solution decreased in proportion with monomer levels as protein adsorbed to microparticle surfaces for all materials except cellulose and steel. Cellulose microparticles preferentially removed all soluble aggregates from the solution, whereas incubation of mAb with steel microparticles resulted in the generation of soluble aggregates. More details of the results for cellulose and steel are reported below.

Theoretical Estimation of mAb Adsorption at Monolayer Coverage

An estimate of the adsorption footprint representing monolayer coverage can be made using Equation 2 using assumptions about the size and orientation of the adsorbedmAb in the calculation:

$$\text{Predicted Adsorption Footprint } (m^2/mg) = \frac{A \times N_A}{(1000M \times \theta_m)} \quad (2)$$

Here, A is projected area of the adsorbed mAb molecule on the surface (m^2), N_A is Avogadro's Number (molecules/mole), M is the molecular weight of the mAb (g/mol), and θ_m is the assumed packing efficiency.

For the projection of a disc of equivalent hydrodynamic diameter (D_h) to the mAb on the surface, the adsorbed area is given by: $A = \pi D_h 2/4$. We calculated the footprint and loading for hexagonal close packing ($\theta_m = 0.91$) or Random Sequential Adsorption (RSA; $\theta_m = 0.547$) of discs on the surface.28 The Random Sequential Adsorption (RSA) model for hard disc monolayer surface adsorption assumes that adsorption is irreversible and random with the constraint that adsorbed discs cannot overlap. For adsorption with a preferential orientation (e.g., end-on or side-on) we can calculate the theoretical coverage based upon approximate mAb molecular dimensions of 10×14×4.5 nm estimated from published crystallographic data.29 One limit is that all the mAb molecules are adsorbed end-on and are perfectly aligned. For random mAb packing but with specific molecular orientation we can use the RSA model28 applied to adsorption of rectangles, where the packing efficiency is about 0.56. The orientations considered were end-on (4.5×14 nm) and side-on (10×14 nm).

A summary of these calculations is given in Table 2. The adsorption footprints of the mAb to the materials tested in this work (given in Table 1) are consistent with mAb monolayer coverage since they were all within the predicted theoretical monolayer from the different models range of 0.27 m^2/mg to 1.1 m^2/mg.

Aggregation of mAb Caused by Stainless Steel Microparticles

Stainless steel adsorbed mAb at levels consistent with a monolayer coverage, but addition of stainless steel microparticles also caused appearance of mAb soluble aggregates in solution. The aggregation caused by passivated stainless steel particles was essentially the same as that for the untreated stainless steel (Figure 3), The fraction of monomer remaining in solution after exposure to particles decreased with increasing amount of stainless steel particles because of the formation of higher order aggregates (Figures 3 and 4). Because we recently demonstrated that soluble tungsten polyanions leached from tungsten particles12 could cause precipitation of this mAb, we also investigated whether potential leachates from a steel microparticle dispersion might exert a similar effect. We found that incubation of the mAb with supernatant obtained from a centrifuged dispersion of stainless steel particles did not change the relative levels of monomeric or dimeric mAb, indicating that leachates from the particles were not responsible for mAb aggregation.

Removal of Soluble mAb Dimers and Soluble Aggregates by Cellulose Microparticles

Surprisingly, addition of cellulose microparticles to a solution of the mAb resulted in a complete removal of the dimer from solution, indicating a preference for the adsorption of dimers over monomer. To investigate this phenomenon further we generated a mAb sample containing about 20% soluble aggregates by heating and agitating a 2 mg/mL mAb solution. This sample was mixed with buffer and a cellulose microparticle dispersion to result in about 0.2 mg/mL total mAb with 6.3 mg/mL cellulose in a 0.5 mL volume. Figure 5 shows

SEC chromatograms of the initial aggregate-containing sample, a sample after 30 min incubation with cellulose, and a sample after 24 hr incubation with cellulose. After 30 min incubation with cellulose, the solution contained 83% of the initial mAb monomer in the sample produced by agitation and heating. The fraction of soluble aggregates was reduced to about 17%. After 24 hr of incubation, 80% of the initial mAb monomer was recovered, and the fraction of soluble aggregates was reduced to about 3%. There was an initial loss of mAb monomer due to adsorption to the cellulose in the first 30 min, but then over the next 24 hr essentially no more monomer was lost. The soluble aggregates continued to decrease upon incubation with the cellulose, suggesting they were removed from solution by multilayer interactions with the mAb-coated cellulose microparticles.

Reversibility of mAb Adsorption

Dilution (in buffer; 10 mM sodium acetate, pH 5.0) of suspensions of mAb adsorbed to glass, cellulose or stainless steel microparticles did not result in greater levels of soluble mAb. In contrast, adsorption was partially reversible after dilution in PBS. With microparticles obtained from glass vials, 63 ± 3 % of the adsorbed mAb was desorbed. With stainless steel microparticles only 7 ± 4 % was desorbed, and with cellulose microparticles 56 ± 6 % was desorbed. Interestingly, the desorbed fraction from cellulose microparticles contained a higher order aggregate that was not present prior to absorption, but which constituted about 0.9% of the desorbed mAb.

Incubation Studies

Incubations of mAb with microparticles composed of glass, cellulose, stainless steel, and Fe_2O_3 were performed using method A in which vials were overfilled with solution so as to eliminate the air-water interface (Figure 6). At the start of the incubation, sufficient amounts of microparticles were added to adsorb about 20% of the mAb. During 30 days of incubation with microparticles from glass vials, syringes, and sulfate-washed vials, the level of mAb monomer in solution did not change (Figure 6, panel A). Dimer and soluble aggregates also remained at constant levels during the incubation (data not shown). We also incubated mAb with silica nanoparticles (data not shown) and silica microparticles (Figure 7) for 5 days without observing measurable mAb monomer loss beyond the initial adsorption or changes in dimer levels (data not shown). With Fe_2O_3 microparticles, the amount of soluble mAb monomer remained essentially constant during the 30-day incubation (Figure 6, panel C), but a minor amount (0.7%) of fragments were detected after 20 days. Incubation of mAb with cellulose resulted in a small but statistically significant ($p = 0.05$) trend of mAb loss over 30 days (Figure 6, panel B). No aggregates were observed in any of the samples containing cellulose.

Incubation of mAb with stainless steel microparticles resulted in a decrease in monomer concomitant with an increase in soluble aggregates (Figure 6, panels C and D). Mass balance analysis confirmed that most of the monomer lost in the first 5 days was converted to soluble aggregates. Subsequently some loss of monomer could be attributed to formation of insoluble aggregates or additional adsorption of monomer to microparticles. For example, after 30 days of incubation the concentration of total soluble species had dropped from an initial value of 0.076 mg/mL to 0.060 mg/mL. Monomer loss from solution was about 40% after 30 days. Passivation of the stainless steel microparticles made no appreciable difference in the results.

The Effect of the Air-Water Interface during Incubation of mAb with Microparticles

In the second incubation method (method B), we investigated the effect of an air-water interface and agitation on the behavior of mAb in the presence of microparticles. During incubation of control samples in the absence of microparticles, there was not a detectable

loss of mAb monomer in the absence of agitation, but agitated samples exhibited a slight loss of soluble monomer (Figure 7). Agitation with headspace of samples containing microparticles of silica, titania or alumina also resulted in slight losses of monomer, but the degree of loss was not greater than that for the agitated control samples with headspace.

Analysis of mAb Secondary Structure Analysis using Infrared Spectroscopy

Figure 8 shows the second-derivative IR spectra for native mAb, boiled mAb, mAb adsorbed to microparticles from glass vials and mAb adsorbed to cellulose microparticles. The bands at 1638 and 1676 cm^{-1} are characteristic of the native β-sheet secondary structure in antibodies.25,30 The bands at 1691 and 1663 cm^{-1} can be assigned to β-turn structures and the peak at 1615 cm^{-1} can be attributed to side-chain absorbance in the native antibody25,30 The spectrum for mAb aggregates prepared by boiling loses the β-sheet peaks characteristic of the native mAb and gains a strong absorbance at 1625 cm^{-1}, attributed to intermolecular β-sheet structures.25,30 Comparison of the adsorbed mAb spectra with the native mAb spectra indicates that the mAb retains near-native secondary structure when adsorbed to glass and cellulose. Similar near-native spectra were obtained for mAb adsorbed to glass syringe microparticles and glass vials microparticles after the ammonium sulfate-wash treatment (not shown).

We were unable to obtain IR spectra of acceptable quality for mAb adsorbed to stainless steel microparticles because the steel particles we used are larger than the cell path length of about 6.5 μm. It has been previously shown that a different mAb had a near-native secondary structure when adsorbed to stainless steel nanoparticles (which could be dispersed within the path length of the IR cell).13 Our attempts to obtain an IR spectrum of mAb adsorbed to steel microparticles using an attenuated total reflection geometry did not yield results of acceptable quality. In this work we used microparticles rather than nanoparticles because we wanted to avoid effects due to the potentially anomalous reactivities of nano-sized particles.

Analysis of mAb Tertiary Structure using Tryptophan Fluorescence Quenching

At low acrylamide concentrations the Stern-Volmer data for mAb adsorbed to glass vials, glass syringes, and cellulose microparticles essentially overlaid the data for the native mAb in solution (Figure 9). For multi-tryptophan proteins (this mAb has 26 Trp), the initial slope of the Stern-Volmer plot can be used to obtain the Stern-Volmer constant.31,32 The Stern-Volmer plot for the unfolded mAb has a much steeper slope than that for either the protein adsorbed to microparticles or the native protein in solution (Table 3). The mAb adsorbed to glass syringes was quenched more that when adsorbed to the other materials but the level of quenching was still low compared with the unfolded protein. The plot for mAb-on-silica exhibits a subtle upward curvature at higher acrylamide concentrations (Figure 9). This upward curvature can result from static quenching at higher quencher concentrations, possibly because of an increase in dynamic flexibility of the protein that allows the quencher to diffuse more readily into the protein interior.31 Incubation of the adsorbed protein for up to five days did not result in a significant change in the K_{SV} for mAb adsorbed to silica microparticles. Therefore this mAb retains a near-native tertiary structure upon adsorption to glass, cellulose, and silica. The mAb adsorbed to silica also remains conformationally stable for at least 5 days. We could not obtain quenching data for mAb adsorbed to stainless steel because no emission signal was observed, consistent with static quenching due to the formation of a ‘dark’ complex between the mAb and the steel.27 This static quenching could be due to unfolding or energy transfer without fluorescence from the Trp to the stainless steel.

DISCUSSION

Incubation of mAb with Microparticles

Over the course of 30 days of incubation, none of the glass microparticles we tested caused loss of mAb monomer beyond the level that was initially adsorbed. Likewise, neither cellulose nor Fe_2O_3 microparticles caused aggregation of the mAb after 30 days. After the initial mAb adsorption to cellulose, there was a small additional loss observed after 30 days incubation. This additional mAb loss upon incubation with cellulose was barely significant ($p<0.05$). We observed a small amount of mAb fragmentation in the presence of Fe_2O_3 microparticles, but the quantity of particles required to produce detectable fragmentation was much greater than that which might be expected to be present in actual formulations. Stainless steel, however, did cause mAb aggregation.

The concentration of soluble aggregates induced by exposure to stainless steel microparticle surfaces increased during incubations, and after extended incubation some insoluble aggregates were also formed. Our results for protein adsorption to steel microparticles are slightly different than those reported by Tyagi *et al.* who found that steel nanoparticles rapidly nucleated large multilayered proteinaceous particles (or possibly agglomerates of mAb-covered primary particles) when incubated with a mAb in a phosphate-buffered formulation containing a non-ionic surfactant at pH 6.13 The minor differences between our studies could be protein-, stainless steel material-(microparticles vs. nanoparticles), or formulation-dependent.

Footprint of mAb Adsorbed on Microparticles

Our results documented that a range of hydrophilic materials could adsorb this mAb in 10 mM sodium acetate buffer (pH 5.0). We did not study mAb adsorption to hydrophobic materials. There are many published reports discussing the adsorption capacity of a wide range of different materials for IgG and some investigations of adsorbed IgG structure under various solution conditions that have largely focused on physiological conditions of pH and ionic strength.30,33–44 But there has not been a comprehensive study of IgG interactions with microparticles of materials and solution conditions likely to be found in therapeutic protein products.

Depending on the packing, order, and surface orientation, monolayer coverage of a mAb on a surface may correspond to a wide variety of adsorption footprints. All of our measured footprints fall within the range that can be estimated from various models (tabulated in Table 2). Based on the rapid adsorption of mAb that we observed to all surfaces except alumina nanoparticles, we expect that the RSA model, which assumes random orientations, would best describe the initial adsorption event. Indeed, the footprint values for mAb adsorption on glass, silica, titania and alumina microparticles were all close to the value predicted using the RSA adsorption model for discs.

In contrast, the footprints for mAb on cellulose were lower than could be explained by monolayer adsorption using the RSA model. The footprint on cellulose corresponds roughly with the size expected from highly ordered, end-on close packing, but the very rapid adsorption and irreversibility of adsorption on cellulose argue against this model. Instead, a more likely explanation may be random adsorption in multiple layers. The observed footprint for the mAb on cellulose roughly corresponds to that expected for a double layer of adsorbed protein.

When the mAb adsorbs on stainless steel, the observed footprint is larger than that predicted by the random sequential adsorption model. A possible explanation for this may be (partial) unfolding of the mAb on the stainless steel surface. This interpretation would be consistent

with the observation that stainless steel microparticles were the only solid surfaces tested in this study that induced aggregation of the mAb during incubation studies.

When the mAb adsorbed to Fe_2O_3, a footprint similar to that observed for adsorption to stainless steel was observed, yet no aggregation of the mAb was observed beyond the initial adsorption event. Although we cannot offer a definitive reason for this observation, it may be possible that, due to agglomeration of microparticles, the surface area reported by nitrogen BET measurement was higher than that which was available for mAb adsorption in the liquid suspensions. The ζ-potential of the Fe_2O_3 microparticles (−2 mV) indicated that the suspension was the least colloidally stable (and thus most likely to agglomerate) microparticle suspension that we tested.

Effect of Microparticle Charge and Size on mAb Adsorption

Proteins may interact with surfaces through attractive dispersion forces and favorable electrostatic forces (if oppositely charged).45 Electrostatic interactions are thought to be a major factor in the binding of proteins to hydrophilic surfaces, so we measured the ζ-potentials of both the particles and the protein. Binding of proteins to surfaces may also be driven by entropy increases arising from changes in protein chain conformations upon adsorption or from displacement of water from hydrophobic surfaces upon adsorption.45

The mAb (pI = 8.7) has a ζ-potential of +12.1 ± 0.4 mV in 10 mM sodium acetate buffer, pH 5.0. In this study we examined mAb binding to hydrophilic surfaces with surfaces charges that were opposite, the same, or relatively neutral relative to the mAb charge. For example, silica, titania and alumina microparticles have surface charges (in 10 mM sodium acetate buffer, pH 5.0) that are very negative, almost neutral, and very positive, respectively. Yet this mAb adsorbed to each of these surfaces. Therefore, the relative surface charges of particles and this mAb (inferred from their respective ζ-potentials) cannot be used to predict the adsorption of this mAb to the hydrophilic surfaces we tested. We interpret this to mean that this mAb fits into the category of a “soft” protein that is capable of adsorbing to a surface of the same charge because there is a gain in entropy by some loss of ordered structure (partial unfolding) after adsorption.45 Theoretically a protein with a “labile” structure could adsorb to all surfaces to some extent.45 On a practical level, our results suggest that it would not be possible to eliminate mAb adsorption by using a container with an opposite surface charge. However, manipulation of the protein charge through solution pH could be used to minimize binding to some surfaces, as shown by the desorption from glass surfaces of some protein when the buffer was changed to PBS. The adsorption of mAb to the near-neutral surface of stainless steel, accompanied by the irreversibility of this binding upon redispersion in PBS suggests that there is an extremely strong binding interaction with stainless steel. We speculate that the reason for this could be surface unfolding due to either hydrophobic interactions with the steel or oxidation of the mAb by the surface followed by conformational changes in the mAb. More work with stainless steel is needed to more fully determine the details of how it induced aggregation of this mAb.

The mAb did not adsorb to alumina nanoparticles but did adsorb to alumina microparticles, even though the ζ-potentials were similar for the two materials. The particle size and SEM data for the alumina nanoparticles are consistent with an agglomerated state, which might at least partially explain the apparent lack of adsorption because in this case the accessible surface area in solution may be much lower than that expected based upon the dry nitrogen adsorption measurements.

Structure of Adsorbed mAb

The mAb secondary structure as determined by IR was near-native when adsorbed to glass and cellulose, and the tertiary structure of mAb on glass, cellulose and silica was near-native as determined by fluorescence quenching. The structure on stainless steel could not be verified using the spectroscopic techniques used in this work. Since our incubation results show that steel caused aggregation of this mAb and aggregates are comprised of protein molecules with perturbed structure, it is logical to conclude that steel caused a structural change in the mAb molecules that resulted in aggregation. We can speculate that the mechanism of steel-induced aggregation is related to the surface chemistry of stainless steel which is rich in chromium oxide. A reasonable hypothesis is that oxidation of adsorbed mAb by the chromium oxide-rich surface of the stainless steel fosters structural changes in adsorbed protein molecules, leading to aggregation. Alternatively it could be unfolding of the adsorbed proteins that leads to aggregation in the bulk. More work is needed to evaluate these hypotheses.

Our results are consistent with previous reports of IgGs retaining near-native secondary structure when adsorbed to silica, alhydrogel (hydrated aluminum hydroxide) and stainless steel.13,26,30 For cellulose, our calculations suggest the adsorbed mAb may be double-layered, yet there is no indication of substantial perturbation in the secondary structure as determined by IR spectroscopy. In a previous report of adsorption to stainless steel nanoparticles, the secondary structure of another mAb was near-native.13 In our work with larger stainless steel microparticles, we observed mAb aggregation, which suggests that the mAb might be unfolding on the microparticle surface.

Influence of Air-water Interfaces on Aggregation of mAb during Incubation

During incubation of mAb with silica microparticles, no aggregation beyond the initial adsorption could be attributed to the microparticles. Rather, the observed loss of monomer resulted from exposure of the mAb to the air-water interface in vials with headspace. There was no synergistic effect of the air-water interface and silica microparticles on mAb aggregation, since mAb exposed to equivalent air-water interfaces aggregated equally in the presence and absence of silica microparticles.

The geometry of the vial can be used to estimate the oscillation in air-water interfacial surface area in vials with headspace as the vial rotated. Based on an area oscillation (normalized to the volume) resulting from rotation of the vials, we estimate that the turnover in air-water interface was about 80 $cm^2mL^{-1}min^{-1}$. In our studies with added silica, we added silica microparticles sufficient to provide a silica-water interfacial area of 135 cm^2/mL. Thus, after 5 days of incubation, the cumulative air-water interface exposure per volume of solution is about 4000-times more than the exposure to the silica interface.

Front-Face Fluorescence Quenching as a Probe of the Tertiary Structure of Adsorbed Proteins

In this work we demonstrated that the tertiary structure of mAb adsorbed to microparticles can be probed by combining front-face fluorescence with collisional quenching. Previously, total internal reflection (TIRF) has been used with quenching to infer the structure of protein adsorbed to a flat silica surface,48 and front-face fluorescence has been used to study highly concentrated mAb solutions49 and lyophilized protein formulations.50 The method described here differs from preceding work in that we used the front-face geometry to collect fluorescence quenching data from opaque dispersions of microparticles. The theory of front-face fluorescence, and comparison with 90° geometry measurements, is given by Eisinger and Flores.51 Front-face measurements are best-suited for opaque samples, and 90° geometry measurements for optically clear dilute samples with a low absorbance.51 The

condition for front-face measurements is that the sample is opaque, expressed by the relation $A_T t \gg 1$, where A_T is the total absorbance of the sample and t is the cell thickness,51 specifically all of the incident light should be absorbed at a sample depth less than the cell thickness. This condition for front-face measurements is valid for opaque particle dispersions but not for dilute solutions without particles.

The initial slopes of the Stern-Volmer plots essentially overlaid for the native mAb in solution and for mAb adsorbed to glass, cellulose and silica microparticles. Therefore, we concluded that the protein tertiary structure was near-native, but possibly slightly perturbed by adsorption to these microparticles. Adsorption of the mAb on stainless steel resulted in a complete static quenching of the fluorescence, possibly indicating that the mAb structure was more perturbed on the steel surface or that energy transfer was occurring without fluorescence. We anticipate that this technique has promise as a tool for evaluating the relative tertiary structure of other proteins bound to surfaces of interest such as those presented by aluminum salt adjuvants.

Formulation Screening with Foreign Microparticles

In order to identify rapidly interactions that may negatively affect the expiry of a therapeutic protein, and to compare different candidate formulations, protein formulations are routinely incubated under conditions where additional stress is applied. Some examples of stress factors include: elevated temperature, freeze-thaw cycles, agitation, and exposure to light.52 However, accelerated studies conducted over a few days are often not predictive of the long-term storage stability of the protein under normal storage conditions.52 One reason for this may be that the accelerated tests do not capture all of the possible degradation pathways that may occur.52 We know that protein interactions with surfaces play an important role in product stability and that otherwise stable proteins may be destabilized by interactions with surfaces.5,52 In this work we found that stainless steel caused mAb aggregation and that cellulose preferentially adsorbed mAb soluble aggregates from solution, and these results could be observed within 30 minutes when the particles were spiked at levels several orders of greater than expected in a real product. Therefore, we propose that the protocol described in this work (method A) can be adapted (for studies of a few hours and/or days) to rapidly assess the sensitivity of formulated proteins to exposure to surfaces of different materials. Furthermore, the combination of adsorption to microparticles and agitation (Method B) can be used to ascertain if these two stresses are synergistic to a given protein.

Because we are proposing the use of this protocol as a protein preformulation stability screening tool, it is useful to evaluate how the relative surface exposure in this protocol compares with estimates of wetted container surface area and the possible foreign particulate levels in a product. In our accelerated incubation studies the added area from microparticles ranged from about 60 to 200 cm^2/mL. For comparison, we estimate that a typical glass vial or syringe with a surface area of about 7 cm^2 would adsorb about 1 μg of mAb based upon our footprint results. Ahalf-inch 25 gauge needle with a wetted inner surface area of less than 0.1 cm^2 would adsorb only about 10 ng of mAb. Therefore we added microparticles surface area at levels on the order of about 10 times (for glass) and 1000 times (for steel) more than an estimate of the fixed surface area (vial, needle) in a pre-filled syringe. There may also be sub-visible foreign particles in the formulation itself, but the surface area contributed by smaller particles is harder to estimate accurately. Tyagi *et al.* estimated that a commercial positive displacement piston filler pump could shed more than 10^4 particles/mL sized around 0.4μm.13 We calculate this particle level would be equivalent to about 5×10^{-5} cm^2 of foreign particle surface area. This surface area could adsorb on the order of 0.02 ng of mAb assuming monolayer adsorption on cellulose, glass or stainless steel. Therefore, our accelerating factor was the addition of on the order of 10^6 times more free-floating particulate contamination surface area to the protein formulation than would be expected in

an actual product. In the same way vigorous agitation is used to rapidly assess the stability of the formulation with respect to transportation stresses, we suggest that addition of foreign particle surface area can rapidly assess sensitivity of protein formulation stability with respect to different potential foreign particulates or wetted surfaces. A question then arises as to how much particulate surface area should be added to obtain an appropriate accelerating factor to identify an adverse interaction of the protein with the surface (e.g. formation of aggregates or degradation products). Because visible aggregate particulates could result from an insignificant loss of protein mass it is difficult to define what amount of aggregation is unacceptable. If we want to perform a stress study that correlates to a 1% aggregation of a product over 2 years (730 days) then (assuming a linear dependence on surface area) addition of 1,000 to 10,000 times more surface area would result in about 1 to 10% of aggregation within a day. This level of acceleration seems appropriate to rapidly identify surfaces that stress the protein formulation. If no adverse effects on the protein formulation (e.g., formation of aggregates or other degradation products) are observed after incubation with a large excess of spiked particulate contamination, protein interactions with that material are unlikely to be a problem at the levels found in real products. Conversely, the appearance degradation products after spiking of particles at very high levels does not necessarily mean that the spiked material would be a problem at the much lower levels of particulate contaminants typically found in real products. For accelerated stability studies with particles more data over a range of stress levels and protein concentrations would be needed to determine the kinetic parameters (rate and order of reaction) in order to make predictions of aggregation rates at particulate levels in real products.

Acknowledgments

Funding for this work was provided by the Graduate Assistantship in Areas of National Need (GAANN) program, the NIH Leadership in Pharmaceutical Biotechnology program (NIH T32 GM008732), the NIH (NIH NIBIB Grant 1 R01 EB006006-01), and Amgen Inc. Thanks to Fredrick G. Luiszer for his help in performing the elemental analyses. Thanks to John Gabrielson and Brent Kendrick for providing access to instrumentation used in some of this work, as well as Linda Narhi, Sampath Krishnan and Robert Platz for scientific discussion and suggestions. Thanks to Dragan Mejic for apparatus design and construction services. This work was performed in part at the University of Colorado's Nanomaterials Characterization Facility.

Abbreviations

mAb	monoclonal antibody
SEC	size exclusion chromatography
UV	ultraviolet

References

1. Schellekens H. Immunogenicity of therapeutic proteins: Clinical implications and future prospects. Clinical Therapeutics. 2002; 24(11):1720–1740. [PubMed: 12501870]
2. Dintzis RZ, Okajima M, Middleton MH, Greene G, Dintzis HM. The Immunogenicity of Soluble Haptenated Polymers Is Determined by Molecular Mass and Hapten Valence. Journal of Immunology. 1989; 143(4):1239–1244.
3. Rosenberg AS. Effects of protein aggregates: An immunologic perspective. Aaps Journal. 2006; 8(3):E501–E507. [PubMed: 17025268]
4. Bachmann MF, Zinkernagel RM. Neutralizing antiviral B cell responses. Annual Review of Immunology. 1997; 15:235–270.
5. Chi EY, Weickmann J, Carpenter JF, Manning MC, Randolph TW. Heterogeneous nucleation-controlled particulate formation of recombinant human platelet-activating factor acetylhydrolase in

pharmaceutical formulation. Journal of Pharmaceutical Sciences. 2005; 94(2):256–274. [PubMed: 15570600]

6. Sharma B. Immunogenicity of therapeutic proteins. Part 2: Impact of container closures. Biotechnology Advances. 2007; 25(3):318–324. [PubMed: 17337336]
7. Sluzky V, Klibanov AM, Langer R. Mechanism of Insulin Aggregation and Stabilization in Agitated Aqueous-Solutions. Biotechnology and Bioengineering. 1992; 40(8):895–903. [PubMed: 18601196]
8. Tzannis ST, Hrushesky WJM, Wood PA, Przybycien TM. Adsorption of a formulated protein on a drug delivery device surface. Journal of Colloid and Interface Science. 1997; 189(2):216–228.
9. Mcleod AG, Walker IR, Zheng S, Hayward CPM. Loss of factor VIII activity during storage in PVC containers due to adsorption. Haemophilia Haemophilia J1 - Haemophilia. 2000; 6(2):89.
10. Jones LS, Kaufmann A, Middaugh CR. Silicone oil induced aggregation of proteins. Journal of Pharmaceutical Sciences. 2005; 94(4):918–927. [PubMed: 15736189]
11. Swift, R.; Nashed-Samuel, Y.; Liu, W.; Narhi, L.; Davis, J. Tungsten, prefilled syringes and protein aggregation. 2007 ACS Meeting; Boston, MA. 2007. (BIOT 15)
12. Bee JS, Nelson SA, Freund E, Carpenter JF, Randolph TW. Precipitation of a Monoclonal Antibody by Soluble Tungsten. Journal of Pharmaceutical Sciences. 2008 in press.
13. Tyagi AK, Randolph TW, Dong A, Maloney KM, Hitscherich C, Carpenter JF. IgG particle formation during filling pump operation: A case study of heterogeneous nucleation on stainless steel nanoparticles. Journal of Pharmaceutical Sciences. 2009; 98(1):94–104. [PubMed: 18454482]
14. Kueltzo LA, Wang W, Randolph TW, Carpenter JF. Effects of solution conditions, processing parameters, and container materials on aggregation of a monoclonal antibody during freeze-thawing. Journal of Pharmaceutical Sciences. 2008; 97(5):1801–1812. [PubMed: 17823949]
15. Ennis R, Pritchard R, Nakamura C, Coulon M, Yang T, Visor G, Lee W. Glass Vials for Small Volume Parenterals: Influence of Drug and Manufacturing Processes on Glass Delamination. Pharmaceutical Development and Technology. 2001; 6(3):393–405. [PubMed: 11485181]
16. Akers, MJ.; Nail, SL. Development and Manufacture of Protein Pharmaceuticals. 1. New York: Kluwer Academic/Plenum Publishers; 2002.
17. Hawe A, Friess W. Formulation development for hydrophobic therapeutic proteins. Pharmaceutical Development and Technology. 2007; 12(3):223–237. [PubMed: 17613886]
18. Ingham E. Host response to biomaterial implants: Biological activity of prosthetic wear particles. Toxicology. 2007; 240(3):137–138.
19. Ingham E, Fisher J. Biological reactions to wear debris in total joint replacement. Proceedings of the Institution of Mechanical Engineers Part H-Journal of Engineering in Medicine. 2000; 214(H1):21–37.
20. Lynch I, Dawson KA. Protein-nanoparticle interactions. Nano Today. 2008; 3(1–2):40–47.
21. Chi EY, Krishnan S, Randolph TW, Carpenter JF. Physical Stability of Proteins in Aqueous Solution: Mechanism and Driving Forces in Nonnative Protein Aggregation. Pharmaceutical Research. 2003; 20(9):1325–1336. [PubMed: 14567625]
22. Standard Practice for Cleaning, Descaling, and Passivation of Stainless Steel Parts, Equipment, and Systems. ASTM A-380-06.
23. Standard Specification for Chemical Passivation Treatments for Stainless Steel Parts. ASTM A-967-05.
24. Glassware - Hydrolytic resistance of the interior surfaces of glass containers - Part 2: Determination by flame spectrometry and classification. ISO 4802–2.
25. Dong A, Huang P, Caughey WS. Protein secondary structures in water from second-derivative amide I infrared spectra. Biochemistry. 1990; 29(13):3303–3308. [PubMed: 2159334]
26. Dong A, Jones LS, Kerwin BA, Krishnan S, Carpenter JF. Secondary structures of proteins adsorbed onto aluminum hydroxide: Infrared spectroscopic analysis of proteins from low solution concentrations. Analytical Biochemistry. 2006; 351(2):282–289. [PubMed: 16460655]
27. Lakowicz, JR. Principles of Fluorescence Spectroscopy. 2. New York: Springer; 1999.
28. Evans JW. Random and Cooperative Sequential Adsorption. Reviews of Modern Physics. 1993; 65(4):1281–1329.

29. Harris LJ, Skaletsky E, McPherson A. Crystallographic structure of an intact IgG1 monoclonal antibody. Journal of Molecular Biology. 1998; 275(5):861–872. [PubMed: 9480774]
30. Giacomelli CE, Bremer MGEG, Norde W. ATR-FTIR Study of IgG Adsorbed on Different Silica Surfaces. Journal of Colloid and Interface Science. 1999; 220(1):13–23. [PubMed: 10550236]
31. Eftink MR, Ghiron CA. Exposure of Tryptophanyl Residues and Protein Dynamics. Biochemistry. 1977; 16(25):5546–5551. [PubMed: 921949]
32. Eftink MR, Ghiron CA. Fluorescence quenching studies with proteins. Analytical Biochemistry. 1981; 114(2):199–227. [PubMed: 7030122]
33. Vermeer AWP, Bremer M, Norde W. Structural changes of IgG induced by heat treatment and by adsorption onto a hydrophobic Teflon surface studied by circular dichroism spectroscopy. Biochimica Et Biophysica Acta-General Subjects. 1998; 1425(1):1–12.
34. Buijs J, White DD, Norde W. The effect of adsorption on the antigen binding by IgG and its F(ab ′)2 fragments. Colloids and Surfaces B: Biointerfaces. 1997; 8(4–5):239–249.
35. Buijs J, Lichtenbelt JWT, Norde W, Lyklema J. Adsorption of monoclonal IgGs and their F(ab′)2 fragments onto polymeric surfaces. Colloids and Surfaces B: Biointerfaces. 1995; 5(1–2):11–23.
36. Buijs J, van den Berg PAW, Lichtenbelt JWT, Norde W, Lyklema J. Adsorption Dynamics of IgG and Its F(ab′)2and Fc Fragments Studied by Reflectometry. Journal of Colloid and Interface Science. 1996; 178(2):594–605.
37. Grabbe ES. Total internal reflection fluorescence with energy transfer: a method for analyzing IgG adsorption on nylon thin films. Langmuir. 1993; 9(6):1574–1581.
38. Kandori K, Miyagawa K, Ishikawa T. Adsorption of immunogamma globulin onto various synthetic calcium hydroxyapatite particles. Journal of Colloid and Interface Science. 2004; 273(2): 406–413. [PubMed: 15082375]
39. Jansson E, Tengvall P. Adsorption of albumin and IgG to porous and smooth titanium. Colloids and Surfaces B: Biointerfaces. 2004; 35(1):45–51.
40. Baszkin A, Boissonnade MM, Kamyshny A, Magdassi S. Adsorption of Native and Hydrophobically Modified Human Immunoglobulin G on Polyethylene Solid Films: Specific Recognition of Adsorbed Layers. Journal of Colloid and Interface Science. 2001; 244(1):18–23.
41. Khamlichi S, Serres A, Muller D, Jozefonvicz J, Brash JL. Interaction of IgG and albumin with functionalized silicas. Colloids and Surfaces B: Biointerfaces. 1995; 4(3):165–172.
42. Galisteo-Gonzalez F, Puig J, Martin-Rodriguez A, Serra-Domenech J, Hidalgo-Alvarez R. Influence of electrostatic forces on IgG adsorption onto polystyrene beads. Colloids and Surfaces B: Biointerfaces. 1994; 2(4):435–441.
43. Bagchi P, Birnbaum SM. Effect of pH on the adsorption of immunoglobulin G on anionic poly(vinyltoluene) model latex particles. Journal of Colloid and Interface Science. 1981; 83(2): 460–478.
44. Lebedeva TS, Rahnanskaya AA, Egorov VV, Pshezhetskii VS. Immunoglobulin adsorption on polymer surfaces. Journal of Colloid and Interface Science. 1991; 147(2):450–456.
45. Norde W. My voyage of discovery to proteins in flatland …and beyond. Colloids and Surfaces B: Biointerfaces. 2008; 61(1):1–9.
46. Norde W, Favier JP. Structure of adsorbed and desorbed proteins. Colloids and Surfaces. 1992; 64(1):87–93.
47. Malmsten M. Formation of Adsorbed Protein Layers. Journal of Colloid and Interface Science. 1998; 207(2):186–199. [PubMed: 9792762]
48. Horsley D, Herron J, Hlady V, Andrade JD. Fluorescence quenching of adsorbed hen and human lysozymes. Langmuir. 1991; 7(2):218–222.
49. Harn N, Allan C, Oliver C, Middaugh CR. Highly concentrated monoclonal antibody solutions: Direct analysis of physical structure and thermal stability. Journal of Pharmaceutical Sciences. 2007; 96(3):532–546. [PubMed: 17083094]
50. Ramachander R, Jiang Y, Li C, Eris T, Young M, Dimitrova M, Narhi L. Solid state fluorescence of lyophilized proteins. Analytical Biochemistry. 2008; 376(2):173–182. [PubMed: 18328251]
51. Eisinger J, Flores J. Front-Face Fluorometry of Liquid Samples. Analytical Biochemistry. 1979; 94(1):15–21. [PubMed: 464277]

52. Randolph TW, Carpenter JF. Engineering challenges of protein formulations. AIChE Journal. 2007; 53(8):1902–1907.

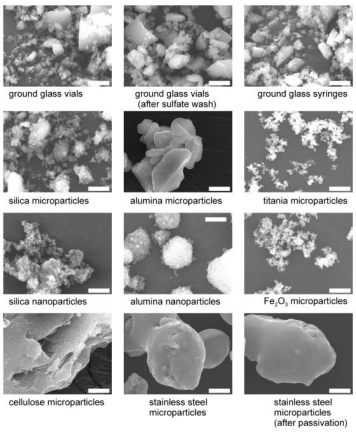

Figure 1.
SEM images of microparticles and nanoparticles used in mAb adsorption studies. The images were all collected at 5000× magnification. The scale bars are 5 μm.

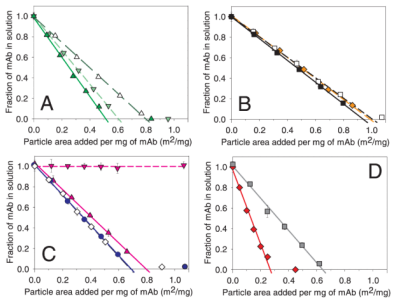

Figure 2.

Adsorption of mAb to particles (numerical footprint values listed in Table 1) Panel A: glass vials (▲); glass syringes (▼); sulfate-washed glass vials (△). Panel B: stainless steel microparticles (■); stainless steel microparticles after passivation treatment (□); Fe_2O_3 microparticles (◆). Panel C: silica microparticles (●); silica nanoparticles (◇); alumina microparticles (▲); alumina nanoparticles (▼). Panel D: cellulose microparticles (◆); titania microparticles (■). We also collected an additional data point, where more microparticles than necessary to adsorb 100% of the mAb were added, to confirm that excess microparticles would remove all of the protein from solution (this data point was not used in the footprint calculation). Data points are means ± SD for separate triplicate samples and lines are regressions of the average data. Error bars may be obscured by symbols. The color version of this figure can be accessed in the online article.

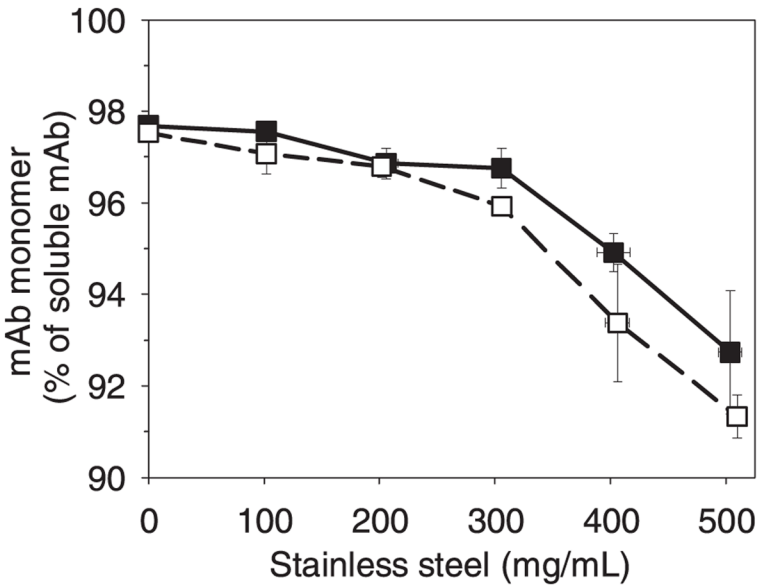

Figure 3.
Decrease in mAb monomer percentage of all soluble species (non-adsorbed mAb) vs. amount of added stainless steel after a 30 minute incubation with 0.1 mg/mL mAb. Legend: stainless steel (■); stainless steel after passivation treatment (□). Data points are means ± SD for separate triplicate samples. Error bars may be obscured by symbols.

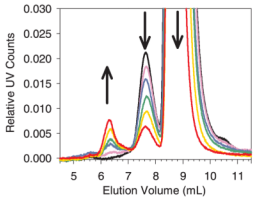

Figure 4.

Zoomed-in view of SEC chromatograms showing the increase in soluble aggregates at ~ 6.3 mL elution volume as a function stainless steel added after a 30 minute incubation with 0.1 mg/mL mAb. The y-axis scale of UV counts was normalized to the control protein monomer peak height. The arrows show the trend in peak height/area as the concentration of stainless steel was increased. This mAb initially contained ~ 2% dimer. The elution of mAb monomer was at ~ 8.7 mL, dimer/soluble aggregates at ~ 7.7 mL and soluble aggregates at ~ 6.3 mL. The baselines were flat from 0 to 5 mL elution volume. Legend: control, black line; 100 mg/mL steel, violet line; 200 mg/mL steel, blue line; 300 mg/mL steel, green line; 400 mg/mL steel, gold line; 500 mg/mL steel, red line. The color version of this figure can be accessed in the online article.

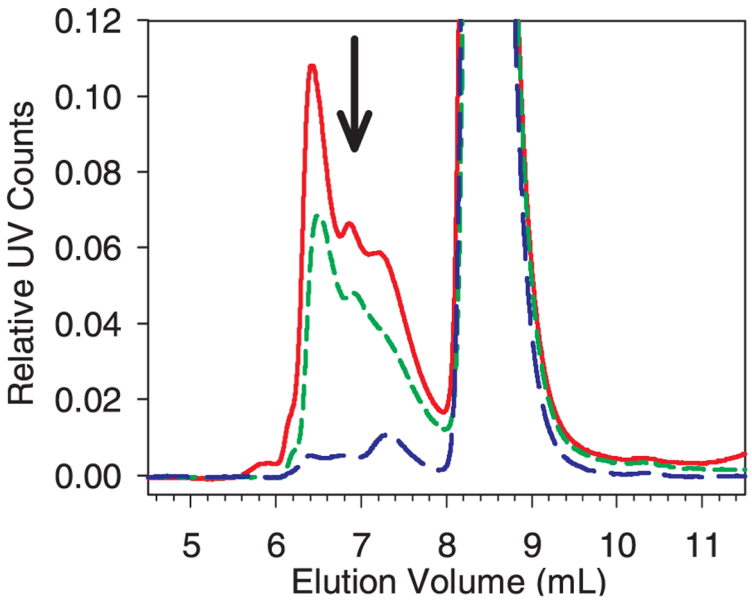

Figure 5.
Zoomed-in view of SEC chromatograms showing the decrease in soluble aggregates when an initially aggregated sample was incubated with cellulose. The y-axis scale of UV counts was normalized to the initial mAb monomer peak height. The arrow shows the trend in peak height/area. Legend: aggregated mAb without added cellulose, solid red line; aggregated mAb after 30 min incubation with cellulose, short-dashed green line; aggregated mAb after 24 hr incubation with cellulose, long-dashed blue line. The color version of this figure can be accessed in the online article.

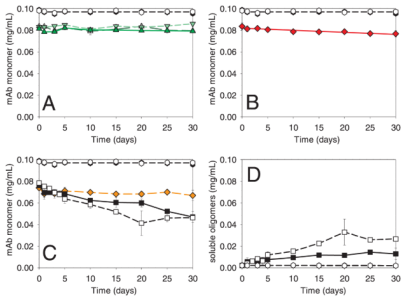

Figure 6.

Incubation of mAb with microparticles in overfilled vials without headspace (method A). Panels A, B and C show mAb monomer as a function of time. Panel D shows soluble aggregates from incubations of mAb with stainless steel. Common to all panels: un-agitated control (μ); agitated control (ν). Panel A: mAb agitated with glass vials (▲); mAb agitated with glass syringes (▼); mAb agitated with sulfate-washed glass vials (△). Panel B: mAb agitated with cellulose (◆). Panel C: mAb agitated with stainless steel (■); mAb agitated with stainless steel after passivation treatment (□), mAb agitated with Fe_2O_3 (◆). Panel D: soluble aggregates after agitation with stainless steel (■); soluble aggregates after agitation with stainless steel after passivation treatment (□). Data points are means ± SD for separate triplicate samples. Error bars may be obscured by symbols. Some symbols may overlay. The color version of this figure can be accessed in the online article.

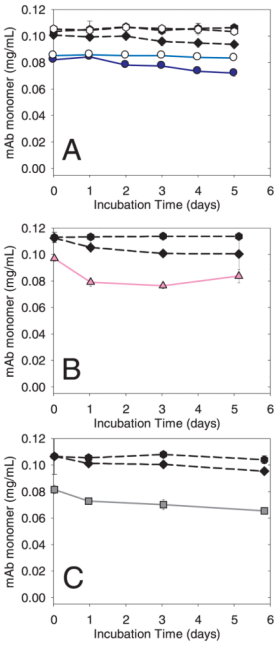

Figure 7.

Incubation of mAb with silica, alumina, and titania. Incubations were performed in vials with headspace (method B). Additional incubations were performed with silica in vials overfilled to minimize the air-water interface (method A). Common symbols in each panel: un-agitated control (μ); agitated control with headspace (◆). Panel A: agitated control without headspace (ν); mAb agitated with silica microparticles with headspace (●); mAb agitated with silica microparticles without headspace (○). Panel B: mAb agitated with alumina microparticles with headspace (▲); Panel C: mAb agitated with titania microparticles with headspace (■). Data points are means ± SD for separate triplicate samples. Error bars may be obscured by symbols. The color version of this figure can be accessed in the online article.

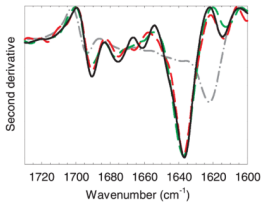

Figure 8.

Second-derivative transmission infrared spectra of mAb adsorbed to particles. Representative spectra from three replicates are shown. Legend: reference native mAb at 23 mg/mL, solid black line; boiled aggregated mAb, gray dot-dash line; mAb adsorbed to glass vials, green long-dash line; mAb adsorbed to cellulose, red medium-dash line. The color version of this figure can be accessed in the online article.

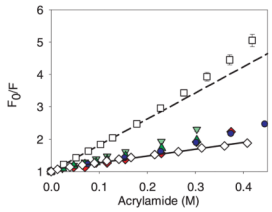

Figure 9.

Stern-Volmer plots for the acrylamide quenching of mAb when free in solution and when bound to microparticles. Legend: native control mAb (◇), with solid line; mAb unfolded in 9 M urea (□), with short dash line; mAb adsorbed to ground glass vials (▲); mAb adsorbed to ground glass syringes (▼); mAb adsorbed to cellulose (◆); mAb adsorbed to silica (●). Data points are mean ± SD for 3 separate experiments. Error bars may be obscured by data points, and some data symbols overlay. The color version of this figure can be accessed in the online article.

Table 1

Summary of particle properties and mAb-particle adsorption footprint values. Particle area was measured by nitrogen adsorption of dry particles. Particle size of microparticles was measured by dilution of a suspension of particles in buffer into pure water in the LS230 laser diffraction particle analyzer. Particle ζ-potential was measured in buffer using the ZetaSizer Nano-ZS®. Adsorption footprints were determined by depletion of protein from solution by addition of particles as described in the methods.

	Particle area (m^2/g ± SD)	Particle size: 90% < size (μm) ; mean size (μm)	Particle ζ-potential (mV ± SD)	mAb adsorption footprint (m^2/mg ± SD)
ground glass vials	5.37 ± 0.03	3.0 ± 0.2 ; 1.0 ± 0.1	−55 ± 2	0.51 ± 0.01
ground glass syringes	5.20 ± 0.03	3.3 ± 0.1 ; 1.1 ± 0.1	−41 ± 1	0.61 ± 0.01
ground glass vials (after sulfate-wash)	7.56 ± 0.01	3.4 ± 0.1 ; 1.3 ± 0.1	−62 ± 2	0.80 ± 0.01
cellulose microparticles	1.91 ± 0.07	23.3 ± 0.4 ; 6.2 ± 0.1	−13 ± 1	0.27 ± 0.03
Fe_2O_3 microparticles	5.0	2 ± 1; 0.7 ± 0.2	−2 ± 15	0.99 ± 0.03
stainless steel microparticles	0.15 ± 0.01	42 ± 1 ; 14 ± 1	−11 ± 1	0.94 ± 0.01
stainless steel microparticles (after passivation)	0.12 ± 0.01	43 ± 1 ; 15 ± 1	−8 ± 2	0.84 ± 0.02
silica microparticles	6.4 ± 0.2	1.4 ± 0.1 ; 0.63 ± 0.02	−42 ± 2	0.69 ± 0.02
silica nanoparticles [a]	73.8 ± 0.1	0.7 [a] (0.015) [a]	−42 ± 1	0.68 ± 0.03
alumina microparticles	0.41 ± 0.01	12.8 ± 0.3 ; 7.6 ± 0.2	+45 ± 1	0.75 ± 0.01
alumina nanoparticles [a]	33.9 ± 0.2	0.5[a] (0.04) [a]	+43 ± 2	NA
titania microparticles	1.9	8.6 ± 0.3 ; 5.0 ± 0.2	−3 ± 1	0.64 ± 0.01

[a]Apparent average size for nanoparticles agglomerates in buffer was measured by dynamic light scattering using the ZetaSizer Nano-ZS® and the manufacturer supplied information for primary nanoparticle size is given in parentheses. Standard deviations represent results from three separate experiments or readings from the same batch/lot of microparticulate material.

Table 2

Summary of theoretical adsorption footprint values and loading of a mAb monolayer adsorbed to a surface for different model scenarios. The models are organized from small to large footprint (high to low in loading). Models considered include: hexagonal close packing of discs (hcp); Random Sequential Adsorption (RSA) of discs and rectangles; and oriented close packing. Equation 2 was used to calculate the footprint values.

Adsorption Model	θ_m	Adsorbed Dimensions	Footprint (m^2/mg)	Loading (mg/m^2)
end-on, close	1	4.5 × 14 nm	0.26	3.8
hcp, disc	0.91	10.5 nm disc	0.40	2.5
end-on, RSA	0.56	4.5 × 14 nm	0.47	2.1
side-on, close	1	10 × 14 nm	0.58	1.7
RSA, disc	0.547	10.5 nm disc	0.66	1.5
side-on, RSA	0.56	10 × 14 nm	1.04	0.96

Table 3

Acrylamide quenching of the tryptophan fluorescence of native, unfolded and adsorbed mAb. The average and standard deviation of three experiments are reported.

	K_{SV} (M^{-1}) ± SD
native mAb control	2.1 ± 0.1
unfolded mAb	8.1 ± 0.3[a]
NATA (free Trp)	23.8 ± 0.8
mAb on ground glass vials	3.1 ± 0.1
mAb on ground glass syringes	4.2 ± 0.3
mAb on cellulose microparticles	3.1 ± 0.1
mAb on silica microparticles	3.2 ± 0.1[a]

[a] K_{SV} taken from initial slope.